Reactions of the Rhenacarborane $[N(PPh_3)_2]_2[Re(CO)_3(\eta^5\text{-}7\text{-}CB_{10}H_{11})]$ with Pentamethylcyclopentadienylrhodium and -iridium Complexes†

John C. Jeffery,‡ Paul A. Jelliss,§ Leigh H. Rees,‡ and F. Gordon A. Stone*,§

Department of Chemistry, Baylor University, Waco, Texas 76798-7348, and School of Chemistry, The University, Bristol BS8 1TS, U.K.

Received January 20, 1998

The rhenium salt $[N(PPh_3)_2]_2[Re(CO)_3(\eta^5\text{-}7\text{-}CB_{10}H_{11})]$ (**1a**) reacts with the group 9 transition-metal complexes $[M(NCMe)_3(\eta^5\text{-}C_5Me_5)][BF_4]_2$ (M = Rh, Ir) to form neutral binuclear metal compounds $[ReM(CO)_3(\eta^5\text{-}C_5Me_5)(\eta^5\text{-}7\text{-}CB_{10}H_{11})]$ (M = Rh (**3a**), Ir (**3b**)). Complex **3a** was characterized by X-ray diffraction as having a $Rh(\eta^5\text{-}C_5Me_5)$ fragment attached to the icosahedral *closo*-2,1-$ReCB_{10}$ framework by a Re−Rh bond and two B−H⇀Rh linkages. The latter involve boron atoms in α- and *β*-sites with respect to the cage carbon atom of the C*BB*BB face of the cage ligating the Re atom. At ambient temperatures, the complex is highly dynamic in solution, although significant exopolyhedral mobility of the $Rh(\eta^5\text{-}C_5Me_5)$ fragment was suppressed by cooling solutions to −88 °C, as determined by a variable-temperature NMR study. Treatment of **3a** with phosphines PR_3 (PR_3 = PMe_3, PMe_2Ph) yields the complexes $[ReRh(CO)_3(PR_3)(\eta^5\text{-}C_5Me_5)(\eta^5\text{-}7\text{-}CB_{10}H_{11})]$ (PR_3 = PMe_3 (**4b**), PMe_2Ph (**5**)). Product **4b** exists only in the form of one green isomer, which contains a B_β−H⇀Rh agostic bond, whereas **5** consists of a mixture of red and green isomers **5a** and **5b**, respectively. Red crystals of **5a** were isolated, and X-ray diffraction revealed that the $\eta^5\text{-}C_5Me_5$ ligand carried by the rhodium atom lies in an anti configuration with respect to the cage carbon atom of the *nido*-7-$CB_{10}H_{11}$ ligand, which is η^5-bound to the rhenium atom. The rhodium atom is also connected to the cage through a B_α−H⇀Rh system, involving a boron atom in a position α to the cage carbon atom of the C*B*BBB face of the cage. In solution, an equilibrium exists between the syn and anti isomers of **5a** and those of the green complex **5b**. The latter contain a B_β−H⇀Rh bonded system. Although **3b** could not be isolated, it could be formed at temperatures below 0 °C and reacted in situ with the phosphines PMe_3 and PMe_2Ph to yield the stable species $[ReIr(CO)_3(PR_3)(\eta^5\text{-}C_5Me_5)(\eta^5\text{-}7\text{-}CB_{10}H_{11})]$ (PR_3 = PMe_3 (**6**), PMe_2Ph (**7**)). For both **6** and **7** it was possible to separate the α- and *β*-isomeric forms by column chromatography to give **6a**/**7a** and **6b**/**7b**, respectively. Complex **6a** was determined by X-ray diffraction to be the anti isomer with a B_α−H⇀Ir bond. In solution, both **6a** and **6b** exist as mixtures of syn and anti isomers. The structure of **7b** determined by X-ray diffraction showed it to have a B_β−H⇀Ir linkage and to be the syn isomer, the only isomeric form in solution, while **7a** had a B_α−H⇀Ir exopolyhedral bond and was a mixture of both syn and anti isomeric species.

Introduction

Relatively few 12-vertex monocarbon metallacarborane complexes have been described[1] since these species were first reported many years ago.[2] Thus, the versatility of [*nido*-7-$CB_{10}H_{11}$]$^{3-}$ as a ligand has hitherto been neglected, a fact which prompted us to prepare the salt $[Na][Pt(PEt_3)_2(\eta^5\text{-}7\text{-}CB_{10}H_{11})]$ and to use it to synthesize dimetal species with Pt−Cu, Pt−Au, and Pt−Hg bonds.[3a] Whereas in the products with Pt−Au and Pt−Hg bonds the *nido*-7-$CB_{10}H_{11}$ group adopts a spectator role in the sense that the carborane cage is solely bonded to platinum in the expected η^5 manner, in the copper−platinum complex, the Pt−Cu bond is augmented by two

† The compounds described in this paper have a rhenium atom incorporated into a *closo*-1-carba-2-rhenadodecaborane structure. However, to avoid a complicated nomenclature for the complexes reported and to relate them to the many known rhenium species with η^5-coordinated cyclopentadienyl ligands, we treat the cages as *nido*-11-vertex ligands with numbering as for an icosahedron from which the twelfth vertex has been removed.

‡ University of Bristol.

§ Baylor University.

(1) Grimes, R. N. In *Comprehensive Organometallic Chemistry II*; Abel, E. W., Stone, F. G. A., Wilkinson, G., Eds.; Pergamon Press: Oxford, U.K., 1995; Vol. 1 (Housecroft, C. E., Ed.), Chapter 9.

(2) Knoth, W. H. *J. Am. Chem. Soc.* **1967**, *89*, 3342. Hyatt, D. E.; Little, J. L.; Moran, J. T.; Scholer, F. R.; Todd, L. J. *J. Am. Chem. Soc.* **1967**, *89*, 3342. Knoth, W. H. *Inorg. Chem.* **1971**, *10*, 598. Rietz, R. R.; Dustin, D. F.; Hawthorne, M. F. *Inorg. Chem.* **1974**, *13*, 1580.

(3) (a) Batten, S. A.; Jeffery, J. C.; Jones, P. L.; Mullica, D. F.; Rudd, M. D.; Sappenfield, E. L.; Stone, F. G. A.; Wolf, A. *Inorg. Chem.* **1997**, *36*, 2570. (b) Blandford, I.; Jeffery, J. C.; Jelliss, P. A.; Stone, F. G. A. *Organometallics* **1998**, *17*, 1402.

S0276-7333(98)00024-7 CCC: $15.00
Publication on Web 04/29/1998

Chart 1

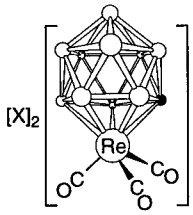

X

1a $N(PPh_3)_2$

1b $NEt_3(CH_2Ph)$

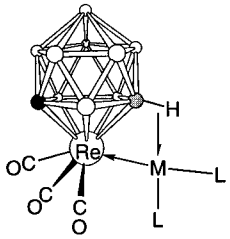

	M	L_2
2a	Pt	$(PPh_3)_2$
2b	Pt	$(PEt_3)_2$
2c	Pt	$Ph_2P(CH_2)_2PPh_2$
2d	Pd	$Ph_2P(CH_2)_2PPh_2$

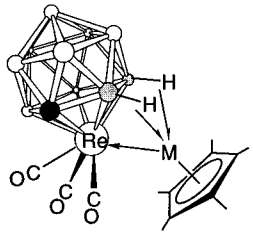

	M
3a	Rh
3b	Ir

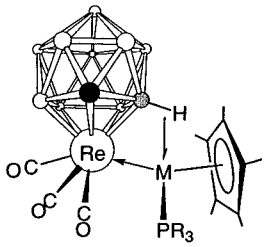

anti isomers shown

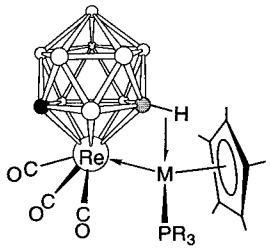

	M	PR_3
4a	Rh	PMe_3
5a	Rh	PMe_2Ph
6a	Ir	PMe_3
7a	Ir	PMe_2Ph

	M	PR_3
4b	Rh	PMe_3
5b	Rh	PMe_2Ph
6b	Ir	PMe_3

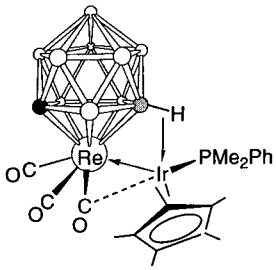

syn isomer only

7b

○ **BH** ◍ **B** ● **CH**

exopolyhedral B−H→Cu linkages formed by B−H vertexes in the CBBBB ring ligating the platinum. We have recently prepared the first monocarbon rhenacarborane $[Re(CO)_3(\eta^5\text{-}7\text{-}CB_{10}H_{11})]^{2-}$ isolating this dianionic complex as the $[N(PPh_3)_2]^+$ (**1a**) or $[NEt_3(CH_2Ph)]^+$ (**1b**) salts, Chart 1.[3b] Studies using **1a** as a synthon have afforded new rhenium−platinum and −palladium complexes $[ReM(CO)_3(PR_3)_2(\eta^5\text{-}7\text{-}CB_{10}H_{11})]$ (M = Pt, R = Ph (**2a**), R = Et (**2b**)) and $[ReM(CO)_3(diphos)(\eta^5\text{-}7\text{-}CB_{10}H_{11})]$ (M = Pt (**2c**), Pd (**2d**), diphos = $Ph_2PCH_2CH_2PPh_2$). In these products, the *closo*-2,1-$ReCB_{10}$ framework forms an exopolyhedral Re−Pt or Re−Pd σ bond while, in addition, there are agostic three-center two-electron B−H→M (M = Pt or Pd) interactions involving B−H vertexes in the CBBBB ring η^5-coordinated to the rhenium. In this paper, we report further studies with the salt **1a** directed toward the synthesis of complexes with Re−Rh and Re−Ir bonds. It was anticipated that these species might reveal novel molecular structures in which rhodium or iridium atoms are exopolyhedrally attached to *closo*-2,1-$ReCB_{10}$ cages both by metal−metal bonds and by B−H→M (M = Rh or Ir) linkages.

Results and Discussion

Treatment of **1a** with $[Rh(NCMe)_3(\eta^5\text{-}C_5Me_5)][BF_4]_2$ in acetonitrile gave the rhenium−rhodium complex **3a**, which on the basis of microanalytical, IR, and NMR data (Tables 1−3) could be formulated as having the composition $[ReRh(CO)_3(\eta^5\text{-}C_5Me_5)(\eta^5\text{-}7\text{-}CB_{10}H_{11})]$. However, such a formulation implies a dimetal species with 30 cluster valence electrons (cve), four short of the number required to give a closed 18-electron shell to each of the metal atoms. Accordingly, an X-ray diffraction study was carried out, the results of which are discussed before the spectroscopic data are reviewed.

The molecular structure of **3a** is shown in Figure 1, and salient bond distances and angles are listed in Table 4. A complication of the structure determination was the fact that **3a** crystallized with three crystallographically independent molecules in the asymmetric unit. All three molecules are structurally akin with Re−Rh bond distances close in magnitude (Re(1)−Rh(1) 2.8345(6) Å, Re(2)−Rh(2) 2.8526(6) Å, Re(3)−Rh(3) 2.8214(6) Å). These parameters all compare well with the Re−Rh distances established in the binuclear metal complexes $[ReRh\{\mu\text{-}\sigma,\eta^5\text{-}7,8\text{-}Me_2\text{-}10\text{-}CH_2(C_6H_4Me\text{-}4)\text{-}7,8\text{-}C_2B_9H_7\}(CO)_4(\eta^5\text{-}C_5H_4Me)]$ (2.888(1) Å)[4a] and $[ReRh(\mu\text{-}CO)_2\{\mu\text{-}Ph_2P(CH_2)PPh_2\}_2(Me)(CO)_2][CF_3SO_3]$ (2.8510(5) Å).[4b] The three rhenium atoms are each bound in an η^5 manner by their respective *nido*-7-$CB_{10}H_{11}$ cages, and all Re−C−O angles are near-linear (Re(1)−C−O average 176.4°, Re(2)−C−O average 176.9°, Re(3)−C−O

(4) (a) Pilotti, M. U.; Stone, F. G. A.; Topaloğlu, I. *J. Chem. Soc., Dalton Trans.* **1991**, 1621. (b) Antonelli, D. M.; Cowie, M. *Organometallics* **1991**, *10*, 2550.

Table 1. Analytical and Physical Data

compd	color	yield/%	ν_{max}(CO)[a]/cm^{-1}	anal./%[b] C	anal./%[b] H
3a [ReRh(CO)$_3$(η^5-C$_5$Me$_5$)(η^5-7-CB$_{10}$H$_{11}$)]	red-brown	81	2026vs, 1962m, 1930s	25.7 (26.3)	4.2 (4.1)
4b [ReRh(CO)$_3$(PMe$_3$)(η^5-C$_5$Me$_5$)(η^5-7-CB$_{10}$H$_{11}$)]	deep green	67	2020vs, 1936s, 1872m	28.3 (28.5)	4.9 (4.9)
5 [ReRh(CO)$_3$(PMe$_2$Ph)(η^5-C$_5$Me$_5$)(η^5-7-CB$_{10}$H$_{11}$)]	red-green[c]	72	2024vs, 1945s, 1868m	31.2 (32.0)	4.5 (4.8)[d]
6a [ReIr(CO)$_3$(PMe$_3$)(η^5-C$_5$Me$_5$)(η^5-7-CB$_{10}$H$_{11}$)] (α)	orange	18	2030vs, 1950s, 1888m	25.5 (25.4)	4.4 (4.4)
6b [ReIr(CO)$_3$(PMe$_3$)(η^5-C$_5$Me$_5$)(η^5-7-CB$_{10}$H$_{11}$)] (β)	purple	73	2022vs, 1938s, 1874m	25.3 (25.4)	4.4 (4.4)
7a [ReIr(CO)$_3$(PMe$_2$Ph)(η^5-C$_5$Me$_5$)(η^5-7-CB$_{10}$H$_{11}$)] (α)	orange	50	2032vs, 1955s, 1920m	29.6 (30.5)	4.2 (4.3)
7b [ReIr(CO)$_3$(PMe$_2$Ph)(η^5-C$_5$Me$_5$)(η^5-7-CB$_{10}$H$_{11}$)] (β)	purple	17	2022vs, 1938s, 1865m	30.5 (30.5)	4.3 (4.3)

[a] Measured in CH_2Cl_2; medium-intensity broad bands observed at ca. 2550 cm^{-1} in the spectra of all the compounds are due to B−H absorptions. [b] Calculated values are given in parentheses. [c] Complex **5a** is red, and **5b** is green (see text); solutions of **5** in CH_2Cl_2 are colored green-brown. [d] Crystallizes with a molecule of CH_2Cl_2.

Table 2. ^{1}H and ^{13}C NMR Data[a]

compd	^{1}H/δ[b]	^{13}C/δ[c]
3a	2.06 (s, 15 H, Me), 2.84 (s br, 1 H, CH)	194.8 (CO), 102.6 (d, *C*$_5$Me$_5$, *J*(RhC) 8), 49.1 (br, CH), 11.1 (C$_5$*Me*$_5$)
4b[d]	−11.56,† −10.70 (m br, 1 H, B−H⇀Rh), 1.47† (dd, 9 H, PMe, *J*(PH) 10, *J*(RhH) < 2), 1.59 (dd, 9 H, PMe, *J*(PH) 11, *J*(RhH) < 2), 1.93† (m, 15 H, C$_5$Me$_5$), 1.94 (d, 15 H, C$_5$Me$_5$, *J*(PH) 4), 2.03, 2.05† (s br, 1 H, CH)	197.7,[e] 197.0 (CO), 105.9† (dd, *C*$_5$Me$_5$, *J*(PC) 6, *J*(RhC) 3), 105.7 (dd, *C*$_5$Me$_5$, *J*(PC) 8, *J*(RhC) 4), 20.5 (d, PMe, *J*(PC) 30), 19.8† (d, PMe, *J*(PC) 29), 11.1, 11.0† (C$_5$*Me*$_5$)
5	−11.26,* −10.47 (m br, 1 H, B−H⇀Rh), 1.50 (d, 3 H, PMe, *J*(PH) 10), 1.59* (d, 15 H, C$_5$Me$_5$, *J*(PH) 4), 1.65 (d, 15 H, C$_5$Me$_5$, *J*(PH) 4), 1.70* (d, 3 H, PMe, *J*(PH) 10), 1.85 (d, 3 H, PMe, *J*(PH) 10), 1.96 (s br, 1 H, CH), 2.00* (d, 3 H, PMe, *J*(PH) 11), 2.11* (s br, 1 H, CH), 7.48−7.54 (m, 5 H, Ph)	197.7, 196.7 (CO), 134.2−129.4 (Ph), 106.2 (dd, *C*$_5$Me$_5$, *J*(PC) 5, *J*(RhC) 2), 106.0* (m, *C*$_5$Me$_5$), 43.4 (br, CH), 20.8 (d, PMe, *J*(PC) 27), 20.3,* 18.2* (d × 2, PMe, *J*(PC) 30 and 28), 13.7 (d, PMe, *J*(PC) 28), 10.7, 10.5* (C$_5$*Me*$_5$)
6a	−13.54 (m br, 1 H, B−H⇀Ir), 1.58 (d, 9 H, PMe, *J*(PH) 10), 1.77* (d, 9 H, PMe, *J*(PH) 10), 2.01* (d, 15 H, C$_5$Me$_5$, *J*(PH) 3), 2.07 (d, 15 H, C$_5$Me$_5$, *J*(PH) 2), 2.10, 2.18* (s br, 1 H, CH)	196.9 (CO), 195.6 (br, CO × 2), 101.9 (d, *C*$_5$Me$_5$, *J*(PC) < 2), 101.8* (*C*$_5$Me$_5$), 47.3, 44.0* (br, CH), 21.1* (d, PMe, *J*(PC) 39), 20.7 (d, PMe, *J*(PC) 38), 10.7, 10.4* (C$_5$*Me*$_5$)
6b[e]	−14.82 (m br, 1 H, B−H⇀Ir), 1.69 (d, 9 H, PMe, *J*(PH) 11), 1.82* (d, 9 H, PMe, *J*(PH) 11), 1.96* (d, 15 H, C$_5$Me$_5$, *J*(PH) 3), 2.04 (d, 15 H, C$_5$Me$_5$, *J*(PH) 2), 2.11 (s br, 1 H, CH)	
7a	−13.30 (m br, 1 H, B−H⇀Ir), 1.54 (d, 3 H, PMe, *J*(PH) 10), 1.64* (d, 15 H, C$_5$Me$_5$, *J*(PH) 3), 1.79 (d, 15 H, C$_5$Me$_5$, *J*(PH) 2), 1.89* (d, 3 H, PMe, *J*(PH) 11), 1.98 (d, 3 H, PMe, *J*(PH) 10), 2.08* (d, 3 H, PMe, *J*(PH) 11), 2.11[f] (s br, 1 H, CH), 7.47−7.56 (m, 5 H, Ph)	195.2[g] (br, CO), 134.4−126.9 (Ph), 102.2* (*C*$_5$Me$_5$), 102.1 (d, *C*$_5$Me$_5$, *J*(PC) 2), 22.3 (d, PMe, *J*(PC) 37), 13.9 (d, PMe, *J*(PC) 36), 10.2, 10.0* (C$_5$*Me*$_5$)
7b	−14.49 (m br, 1 H, B−H⇀Ir), 1.70 (d, 15 H, C$_5$Me$_5$, *J*(PH) 2), 1.88 (d, 3 H, PMe, *J*(PH) 11), 2.02 (d, 3 H, PMe, *J*(PH) 11), 7.44−7.55 (m, 5 H, Ph)	196.6 (CO), 134.3 (d, C^1(Ph), *J*(PC) 56), 131.4 (d, C^4(Ph), *J*(PC) 3), 131.1 (d, C^2(Ph), *J*(PC) 8), 129.2 (d, C^3(Ph), *J*(PC) 11), 102.0 (d, *C*$_5$Me$_5$, *J*(PC) 2), 36.2 (br, CH), 21.5 (d, PMe, *J*(PC) 39), 18.6 (d, PMe, *J*(PC) 36), 10.1 (C$_5$*Me*$_5$)

[a] Chemical shifts (δ) in ppm, coupling constants (*J*) in hertz, measurements in CD_2Cl_2 at room temperature. Peaks marked with an asterisk are due to a minor isomer (see text). [b] Resonances for terminal BH protons occur as broad unresolved signals in the range δ ca. −2 to 3. [c] ^{1}H-decoupled chemical shifts are positive to high frequency of SiMe$_4$. [d] Peaks marked with a dagger (†) are due to the isomeric form of **4b** initially present as a minor species. [e] ^{13}C{^{1}H} NMR spectrum unavailable due to very low solubility of sample. [f] Signal due to cage CH in minor isomer masked by other peaks. [g] Signal due to cage CH not observed due to low solubility.

average 175.2°). In turn, the Rh atoms are ligated by η^5-C$_5$Me$_5$ groups (Rh(1)−C(C$_5$Me$_5$) average 2.162 Å, Rh(2)−C(C$_5$Me$_5$) average 2.151 Å, Rh(3)−C(C$_5$Me$_5$) average 2.154 Å). Of particular importance is the presence in each of the three molecules of two B−H⇀Rh three-center two-electron agostic bonds, the hydrogen atoms of which were located and refined. Without exception, and despite apparent disorder in molecule 2, one of these interactions involves a B$_\alpha$−H bond and the other a B$_\beta$−H bond in the C*BB*BB faces of the cages ligating the rhenium atoms. Hence, all molecules lack a mirror plane of symmetry that they might otherwise have contained if both B−H⇀Rh agostic groups in each complex utilized the two available B$_\beta$−H bonds. As would be expected, there are two short Rh−B distances observed in each independent molecule (Rh(1)−B(12) 2.311(7) Å, Rh(1)−B(13) 2.357(7) Å, Rh(2)−B(22) 2.331(7) Å, Rh(2)−B(23) 2.301(8) Å, Rh(3)−B(32) 2.370(8) Å, Rh(3)−B(33) 2.316(7) Å). As a result of the X-ray diffraction study, it can thus be inferred that **3a** contains a [*nido*-7-CB$_{10}$H$_{11}$]$^{3-}$ ligand making an overall contribution of 7e$^-$ to the dimetal fragment. This donation together with the contributions from the other ligands affords the expected closed shell cve count of 34 for the molecule.

The presence of the two B−H⇀Rh bonds from the CBBBB face of the cage ligating the rhenium atom in **3a** deserves further comment in the context of the earlier characterization of numerous dimetal complexes of the transition elements having [*nido*-7,8-R$_2$-7,8-C$_2$B$_9$H$_9$]$^{2-}$ (R = H or Me) ligands bridging the metal−metal bonds.[5] In many of these dicarbon carborane structures, the cage contributes six valence electrons to the overall electron count in the molecule, doing so by formally donating four electrons via η^5 bonding to one metal center and donating two electrons via three-center exopolyhedral bonding to the other. Thus, generally one B−H⇀M exopolyhedral bond rather than two exists in the structure. However, both the mono- and dicarbon

(5) (a) Stone, F. G. A. *Adv. Organomet. Chem.* **1990**, *31*, 53. (b) Brew, S. A.; Stone, F. G. A. *Adv. Organomet. Chem.* **1993**, *35*, 135. (c) Jelliss, P. A.; Stone, F. G. A. *J. Organomet. Chem.* **1995**, *500*, 307.

Table 3. ^{11}B and ^{31}P NMR Data[a]

compd	^{11}B/δ[b]	^{31}P/δ[c]
3a	10.3 (1 B), −5.3 (2 B), −9.8 (2 B), −12.7 (1 B), −15.0 (2 B), −18.2 (2 B)	
4b[d]	24.6 (1 B, B−H→Rh), 21.2† (1 B, B−H→Rh), 1.2† (1 B), −1.5 (1 B), −4.4 (1 B), −6.7 (1 B), −8.4 (1 B), −10.0† (1 B), −13.2 (3 B), −15.7 (2 B), −21.4† (2 B)	−11.3 (d, *J*(RhP) 145), −13.1† (d, *J*(RhP) 150)
5	22.5* (1 B, B−H→Rh), 22.0 (1 B, B−H→Rh), 1.8 (1 B), 0.8 (1 B), −1.3* (1 B), −3.3 (1 B), −3.9* (1 B), −6.4* (1 B), −8.8* (1 B), −9.4 (1 B), −13.7 (3 B), −16.0 (2 B), −21.4* (1 B)	12.9* (d, *J*(RhP) 136), 5.8* (d, *J*(RhP) 134), 1.5 (d, *J*(RhP) 149), −0.1* (d, *J*(RhP) 146)[e]
6a	23.4 (1 B, B−H→Ir), 21.3* (1 B, B−H→Ir), 2.8 (1 B), 0.9 (1 B), −1.5 (1 B), −9.1* (1 B), −11.2 (1 B), −14.3 (3 B), −15.9 (2 B), −19.5* (1 B)	−44.8,* −47.2
6b	25.1 (1 B, B−H→Ir), −0.6 (1 B), −3.0 (1 B), −6.5 (1 B), −8.7 (1 B), −12.3 (1 B), −14.7 (2 B), −16.3 (1 B), −21.3 (1 B)	−42.1,* −43.0
7a	25.5* (1 B, B−H→Ir), 24.8 (1 B, B−H→Ir), 3.5 (1 B), 0.5 (1 B), −0.7 (1 B), −10.2 (1 B), −14.2 (3 B), −15.1 (1 B), −16.5 (1 B)	−30.3,* −31.8
7b	24.4 (1 B, B−H→Ir), −0.5 (1 B), −2.9 (1 B), −6.2 (1 B), −9.2 (1 B), −12.0 (1 B), −14.2 (1 B), −14.9 (1 B), −16.3 (1 B), −21.3 (1 B)	−32.5

[a] Chemical shifts (δ) in ppm, coupling constants (*J*) in hertz, measurements in CD_2Cl_2 at room temperature. Peaks marked with an asterisk are due to a minor isomer (see text). [b] ^{1}H-decoupled chemical shifts are positive to high frequency of $BF_3{\cdot}Et_2O$ (external). B−H→M assignments made from fully coupled ^{11}B spectrum. [c] ^{1}H-decoupled chemical shifts are positive to high frequency of H_3PO_4 (external). [d] Peaks marked with a dagger (†) are due to the isomeric form of **4b** initially present as a minor species. [e] Peak integral ratio: 1:10:70:30.

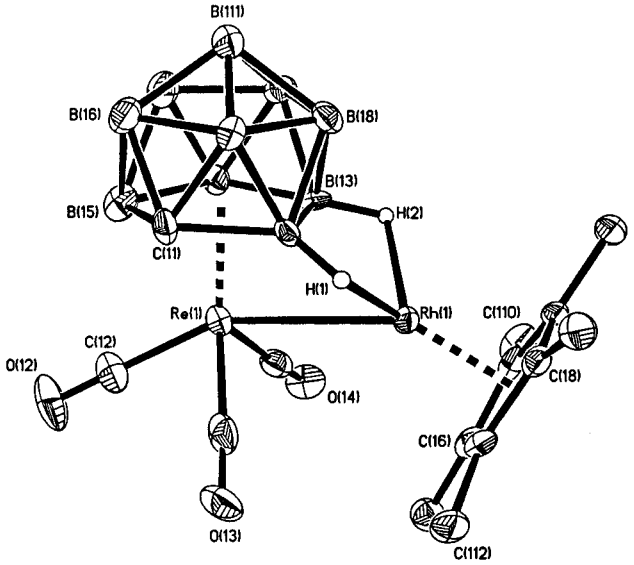

Figure 1. Structure of $[ReRh(CO)_3(\eta^5\text{-}C_5Me_5)(\eta^5\text{-}7\text{-}CB_{10}H_{11})]$ (**3a**), showing the crystallographic labeling scheme. Thermal ellipsoids are shown at the 40% probability level. Only the agostic hydrogen atoms are shown for clarity.

carborane copper complexes $[PtCu(PEt_3)_2(PPh_3)(\eta^5\text{-}7\text{-}CB_{10}H_{11})]$[3a] and $[Cu_2(PPh_3)_2(\eta^5\text{-}7,8\text{-}C_2B_9H_{11})]$[6] have molecular structures with metal−metal bonds and two B−H→Cu linkages to the exopolyhedral copper atoms.

The IR spectrum of **3a** displayed three ν_{max}(CO) absorbances at 2026vs, 1962m, and 1930s cm^{-1} (Table 1). The compound was extremely soluble in CD_2Cl_2 and gave rise to strong, unambiguous signals in its NMR spectra. The ^{1}H NMR spectrum (Table 2) was relatively simple with just a sharp singlet due to the methyl groups and a broad signal at δ 2.84 characteristic of a cage CH proton,[5b] while the ^{11}B{^{1}H} NMR spectrum (Table 3) revealed a pattern of six peaks (1:2:2:1:2:2). This clearly implies the existence of a mirror plane of symmetry in the molecule in solution, in stark contrast with the results of the X-ray structure determination for the molecule in the solid state. Furthermore, there was no NMR evidence for the B−H→Rh linkages which routinely manifest themselves as broad multiplets in the ^{1}H NMR spectrum in the range from δ −5 to −12, sometimes with resolved ^{11}B−^{1}H quartet coupling (*J*(BH) = 60−90 Hz).[5b] The *B*−H→M boron nuclei invariably give rise to low-field doublets (δ 10−30) with a diminished ^{1}H−^{11}B coupling constant (*J*(HB) = 60−90 Hz). For complex **3a**, all signals in the fully coupled ^{11}B NMR spectrum appear as doublets with *J*(HB) > 100 Hz. In particular, the doublet at δ 10.3, which borders on the accepted chemical shift range for B−H→M agostic systems, has a ^{1}H−^{11}B coupling of 131 Hz, which far exceeds the expected value for a three-center B−H→M group.[5b] The ^{13}C{^{1}H} NMR spectrum was strong and informative, with doublet and singlet peaks arising from pentamethylcyclopentadienyl ring (δ 102.6 (d, *J*(RhC) = 8 Hz)) and methyl (δ 11.1) carbon nuclei, respectively, and a diagnostic broad peak for the cage-carbon nucleus at δ 49.1. The carbon nuclei of the CO ligands give rise to only one sharp singlet resonance at δ 194.8.

On the basis of these data, two scenarios are envisaged. First, and at the very least, an isomerization process is occurring in solution at ambient temperatures, which involves rapid exchange of the adjacent $B_{\alpha/\beta}$−H bonds in the coordinating CBBBB face of the cage involved in the B−H→Rh linkages (Scheme 1). Generation of the $\beta\beta'$ isomer along the isomerization pathway is sufficient to produce a mirror plane in the complex, which could account for the observed ^{11}B{^{1}H} NMR spectrum at ambient temperatures. A similar mechanism was proposed to account for the dynamic NMR spectra of the complex $[RePd(CO)_3(diphos)(\eta^5\text{-}7\text{-}CB_{10}H_{11})]$ (**2d**).[3b] In this complex, there is only one B−H→Pd moiety in the ground-state structure and the minimal requirement for production of the pseudomirror plane of symmetry in **2d** is a fast exchange between alternative B_β−H bonds involved in exopolyhedral bridging to the palladium atom. However, this process is not enough to make all three carbonyl carbon nuclei in **2d** equivalent (δ(CO) 196.9 (CO × 1), 194.0 (CO × 2)). Similarly, the proposed exchange of $B_{\alpha/\beta}$−H and $B_{\alpha'/\beta'}$−H bonds in **3a** (Scheme 1) would also be incapable of rendering all carbonyl ligands equivalent, yet this is what was observed. Thus, a second dynamic event (Scheme 1) may involve heterolytic fission of the Re−Rh bond, followed by rapid migration of the Rh(η^5-C_5Me_5) unit about the polyhedral *closo*-2,1-$ReCB_{10}$ framework by multiple exchanges of B−H bonds employing

Table 4. Selected Internuclear Distances (Å) and Angles (deg) for [ReRh(CO)$_3$(η^5-C$_5$Me$_5$)(η^5-7-CB$_{10}$H$_{11}$)] (3a) with Estimated Standard Deviations in Parentheses

			Molecule 1				
Re(1)−C(14)	1.922(7)	Re(1)−C(13)	1.959(8)	Re(1)−C(12)	1.961(8)	Re(1)−B(12)	2.297(7)
Re(1)−B(15)	2.298(8)	Re(1)−B(13)	2.317(7)	Re(1)−C(11)	2.325(6)	Re(1)−B(14)	2.386(7)
Re(1)−Rh(1)	2.8345(6)	Rh(1)−B(12)	2.311(7)	Rh(1)−B(13)	2.357(7)	Rh(1)−H(1)	1.88(5)
Rh(1)−H(2)	2.03(6)	C(12)−O(12)	1.139(8)	C(13)−O(13)	1.138(8)	C(14)−O(14)	1.156(8)
Rh(1)−C(C$_5$Me$_5$)	average 2.162						
Re(1)−B(12)−Rh(1)	75.9(2)	Re(1)−B(13)−Rh(1)	74.7(2)	O(12)−C(12)−Re(1)	177.9(7)		
O(13)−C(13)−Re(1)	176.3(6)	O(14)−C(14)−Re(1)	174.9(6)				
			Molecule 2				
Re(2)−C(22)	1.938(7)	Re(2)−C(23)	1.941(7)	Re(2)−C(24)	1.964(8)	Re(2)−B(23)	2.283(8)
Re(2)−B(25)	2.292(7)	Re(2)−B(22)	2.309(8)	Re(2)−B(24)	2.341(7)	Re(2)−C(21)	2.354(7)
Re(2)−Rh(2)	2.8526(6)	Rh(2)−B(23)	2.301(8)	Rh(2)−B(22)	2.331(7)	Rh(2)−H(3)	1.87(6)
Rh(2)−H(4)	1.88(6)	C(22)−O(22)	1.158(8)	C(23)−O(23)	1.147(7)	C(24)−O(24)	1.123(8)
Rh(2)−C(C$_5$Me$_5$)	average 2.151						
Re(2)−B(22)−Rh(2)	75.9(2)	Re(2)−B(23)−Rh(2)	77.0(2)	O(22)−C(22)−Re(2)	177.4(6)		
O(23)−C(23)−Re(2)	177.6(5)	O(24)−C(24)−Re(2)	175.7(6)				
			Molecule 3				
Re(3)−C(33)	1.909(7)	Re(3)−C(34)	1.931(8)	Re(3)−C(32)	1.934(7)	Re(3)−B(32)	2.297(7)
Re(3)−B(33)	2.302(8)	Re(3)−C(31)	2.313(7)	Re(3)−B(35)	2.329(8)	Re(3)−B(34)	2.348(8)
Re(3)−Rh(3)	2.8214(6)	Rh(3)−B(33)	2.316(7)	Rh(3)−B(32)	2.370(8)	Rh(3)−H(5)	1.95(6)
Rh(3)−H(6)	1.83(6)	C(32)−O(32)	1.151(8)	C(33)−O(33)	1.164(7)	C(34)−O(34)	1.154(8)
Rh(3)−C(C$_5$Me$_5$)	average 2.154						
Re(3)−B(32)−Rh(3)	74.4(2)	Re(3)−B(33)−Rh(3)	75.3(2)	O(32)−C(32)−Re(3)	177.5(6)		
O(33)−C(33)−Re(3)	172.7(6)	O(34)−C(34)−Re(3)	175.3(6)				

Scheme 1. Dynamic Processes in Complex 3a[a]

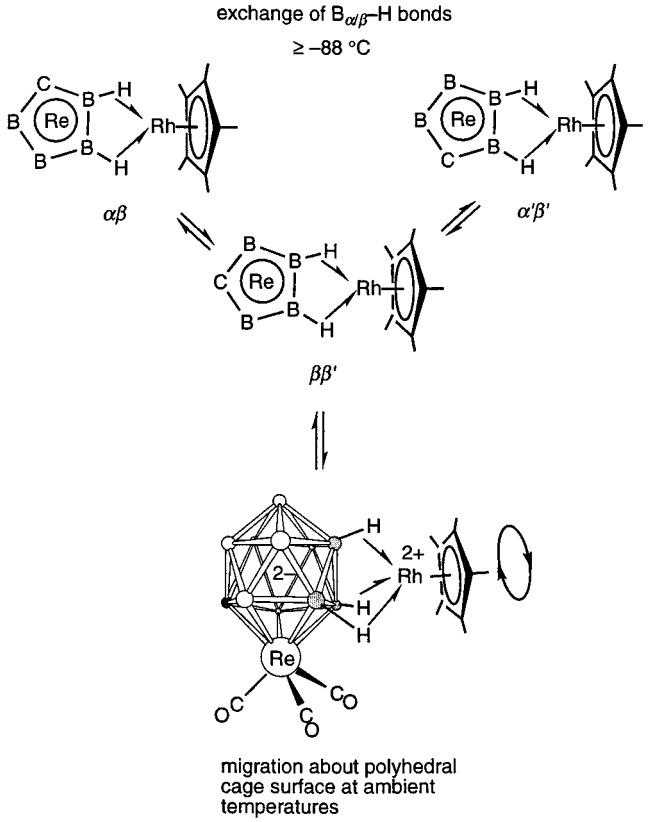

[a] Part of the cage is omitted in some molecules for clarity.

a maximum of three B−H⇀Rh bonds, involving B−H vertexes both in the coordinating lower CB_4 and the upper B_5 pentagonal belts. This would leave a Re(CO)$_3$ unit bound to the CBBBB cage face, effectively giving a zwitterionic complex. The Re(CO)$_3$ moiety must be spinning rapidly relative to the remainder of the *nido*-7-$CB_{10}H_{11}$ group about an axis along the Re atom and the centroid of the CBBBB ligating face, a process which

Table 5. Variable-Temperature ^{1}H and ^{13}C{^{1}H} NMR Study on Complex 3a

T/°C	δ(Me)[a]	δ(CH)[a]	$\nu_{1/2}$(CH)[b]/Hz	δ(CO)[c]
22	2.06	2.82	12	194.8
−38	2.03	2.79	35	
−88	2.02	2.78	11	194.0, 193.9 (1:2)

[a] ^{1}H NMR spectral data. [b] Peak line width. [c] ^{13}C{^{1}H} NMR spectral data.

occurs in the parent complex **1a**.[3b] In this manner, local C_{3v} symmetry is generated with respect to the CO ligands, giving rise to the observation of one CO carbon resonance in the ^{13}C{^{1}H} NMR spectrum. Very similar dynamic exchange processes have been documented for the complexes [*exo*-5,10-{Rh(PPh$_3$)$_2$}-5,10-μ-(H)$_2$-*endo*-10-X-7,8-Me$_2$-*nido*-7,8-$C_2B_9H_7$] (X = H,[7a] Au(PPh$_3$)[7b]). In these species, the Rh(PPh$_3$)$_2$ fragment traverses the B−H vertexes in an exopolyhedral manner, scrambling about the polyhedral cage surface both at ambient and at low (−80 °C) temperatures in solution, i.e., the fluxionality could not be "frozen" out at the lowest temperatures measured. A variable-temperature ^{1}H NMR study of **3a** revealed an interesting change in the signal due to the cage CH proton (Table 5) as the temperature is lowered to −88 °C. The signal broadens to a maximum value $\nu_{1/2}$ = 35 Hz at ca. −38 °C and then sharpens as the temperature is lowered further to −88 °C ($\nu_{1/2}$ = 11 Hz). This is accompanied by a slight change in chemical shift, along with a small but perceptible variation for the methyl protons. The change in C*H* peak width is indicative of a solution process which has been subdued. It was notable that the ^{1}H NMR spectrum at −88 °C did not show the presence of a B−H⇀Rh system, with the expected diagnostic broad high-field resonance(s). Thus, the

(6) Kang, H. C.; Do, Y.; Knobler, C. B.; Hawthorne, M. F. *Inorg. Chem.* **1988**, *27*, 1716.
(7) (a) Long, J. A.; Marder, T. B.; Behnken, P. E.; Hawthorne, M. F. *J. Am. Chem. Soc.* **1984**, *106*, 2979. (b) Jeffery, J. C.; Jelliss, P. A.; Stone, F. G. A. *J. Chem. Soc., Dalton Trans.* **1993**, 1073.

species in solution at this temperature cannot be equated with the solid-state structure, which, as discussed previously, contains two B−H⇀Rh bonds. It would appear that the migration of the Rh(η^5-C_5Me_5) group about the *closo*-2,1-$ReCB_{10}$ framework has been frozen out with a Re−Rh bond probably in place at −88 °C. However, the exchange of B−H bonds in the (B−H⇀Rh)$_2$ system ($\alpha\beta \leftrightarrow \beta\beta' \leftrightarrow \alpha'\beta'$, Scheme 1) must still be occurring. The $^{13}C\{^1H\}$ NMR spectrum measured at −88 °C verifies this by revealing two peaks due to the carbonyl carbon nuclei at δ 194.0 (CO × 1) and 193.9 (CO × 2). The generation of a pseudomirror plane encompassing the Re, Rh, and cage C atoms and the CO ligand transoid to the Rh atom is therefore confirmed. It is possible that the species at low temperature is the static $\beta\beta'$ isomer (Scheme 1), which contains a permanent mirror plane, but this is unlikely for two reasons: (i) as mentioned, no B−H⇀Rh protons could be detected in the ^1H NMR spectrum at this temperature, and (ii) such a static structure, were it to exist in solution, might be expected to correspond to that observed in the X-ray structure (Figure 1), i.e., the unsymmetrical $\alpha\beta$ isomer.

An attempt to use the same preparative methodology to isolate and fully characterize an analogous rhenium−iridium complex $[ReIr(CO)_3(\eta^5\text{-}C_5Me_5)(\eta^5\text{-}7\text{-}CB_{10}H_{11})]$ (**3b**) did not succeed. However, **3b** could be formed at temperatures below 0 °C by treatment of **1a** with $[Ir(NCMe)_3(\eta^5\text{-}C_5Me_5)][BF_4]_2$ in CH_2Cl_2. An IR spectrum of an aliquot taken from the solution at −30 °C showed a pattern of ν_{max}(CO) absorptions very similar to those for **3a** with peaks at 2026vs, 1954m, and 1918s cm^{-1}. If allowed to warm to room temperature, solutions of **3b** decomposed. Nevertheless, it was deemed probable that **3b** could still be a useful reagent if produced and reacted in situ at or below 0 °C. Results employing this reagent will be discussed after reactions of **3a** with phosphines are presented.

Treatment of **3a** with 1 equiv of PMe_3 at −10 °C yielded a green complex $[ReRh(CO)_3(PMe_3)(\eta^5\text{-}C_5Me_5)(\eta^5\text{-}7\text{-}CB_{10}H_{11})]$ (**4b**). The IR spectrum of **4b** is straightforward (Table 1) with ν_{max}(CO) absorptions at 2020vs, 1936s, and 1872m cm^{-1} and gives no hint of the complications arising from the possibility of the presence of different isomers. Before the NMR data and specific structure for **4b** can be rationalized, it is informative to discuss the reaction of **3a** with 1 equiv of PMe_2Ph. This gave a mixture of green and red compounds which could be separated on a chromatography column. However, within minutes in solution, the fractions reverted to mixtures of identical proportions. The red and green complexes are clearly in equilibrium in solution. After microanalytical, IR (Table 1), and NMR data (Tables 2 and 3) were obtained, the mixture was formulated as having the composition $[ReRh(CO)_3(PMe_2Ph)(\eta^5\text{-}C_5Me_5)(\eta^5\text{-}7\text{-}CB_{10}H_{11})]$ (**5**). Both green and red crystals were grown from the mixture; those of the green complex were regrettably intractable, but the red crystals were suitable for X-ray diffraction analysis. The structure is shown in Figure 2 and is designated as **5a**-*anti* because of the relative disposition of the η^5-C_5Me_5 group and the cage C(1) atom, a feature discussed further below. Selected bond lengths and angles are given in Table 6.

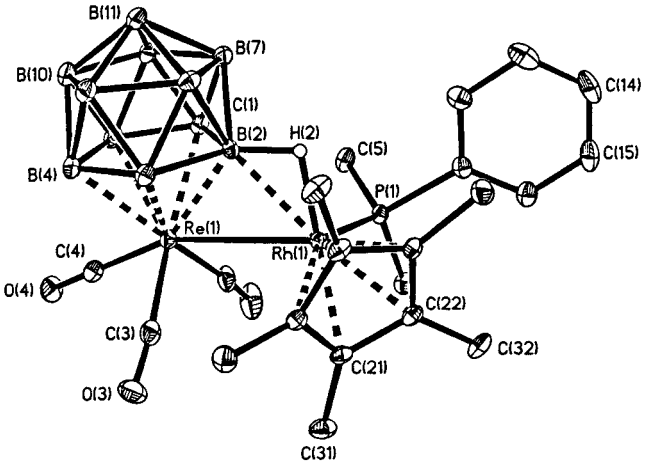

Figure 2. Structure of $[ReRh(CO)_3(PMe_2Ph)(\eta^5\text{-}C_5Me_5)(\eta^5\text{-}7\text{-}CB_{10}H_{11})]$ (**5a**-*anti*), showing the crystallographic labeling scheme. Thermal ellipsoids are shown at the 40% probability level. Only the agostic hydrogen atom is shown for clarity.

The Re(1)−Rh(1) bond length (2.9821(4) Å) is marginally longer than the distances observed in complex **3a** (average of the three molecules Re−Rh 2.8362 Å) and the structures of $[ReRh\{\mu\text{-}\sigma,\eta^5\text{-}7,8\text{-}Me_2\text{-}10\text{-}CH_2(C_6H_4Me\text{-}4)\text{-}7,8\text{-}C_2B_9H_7\}(CO)_4(\eta^5\text{-}C_5H_4Me)]$ (2.888(1) Å)[4a] and $[ReRh(\mu\text{-}CO)_2\{\mu\text{-}Ph_2P(CH_2)PPh_2\}_2(Me)(CO)_2][CF_3SO_3]$ (2.8510(5) Å).[4b] The Re(1)−Rh(1) bond of **5a**-*anti* is spanned by the *nido*-7-$CB_{10}H_{11}$ cage, which is itself η^5-coordinated through the $\overline{CBBBB}$ face to the rhenium atom (Re(1)−C(1) 2.324(3) Å, Re(1)−B(2) 2.260(3) Å, Re(1)−B(3) 2.363(3) Å, Re(1)−B(4) 2.373(3) Å, Re(1)−B(5) 2.361(3) Å). The Re(1)−B(2) distance is ca. 0.1 Å shorter than the remaining Re−B contacts because of the presence of the bridging B(2)−H(2)⇀Rh(1) agostic bond. This system also results in a B(2)−Rh(1) connectivity of 2.307(3) Å. Thus a B_α−H bond is utilized for three-center two-electron bonding, i.e. the boron atom adjacent to the carbon in the $\overline{CBBBB}$ coordinating face of the cage is involved. The Re−C−O units are all near-linear (Re(1)−C−O average 175.3°). The Rh(1)−P(1) distance (2.3369(8) Å) is very close in magnitude to the average found for a range of Rh−PMe_2Ph bonds (2.325 Å).[8] The η^5-C_5Me_5 ligand is perceptibly slipped [Rh(1)−C(21) 2.227(2) Å, Rh(1)−C(22) 2.235(2) Å, Rh(1)−C(23) 2.204(2) Å, Rh(1)−C(24) 2.259(3) Å, Rh(1)−C(25) 2.323(3) Å). This is probably in response to the build up of electron density on the rhodium atom due to the ligation of three strong donor groups, viz. PMe_2Ph, B−H⇀Rh, and the η^5-C_5Me_5 ligand itself, in addition to the steric congestion caused by the presence of all of these groups around the Rh(1) atom. However, slippage is insufficient to consider lowering the hapticity of the pentamethylcyclopentadienyl group from η^5. It is important to note that this structure reveals that the η^5-C_5Me_5 ligand bound to the Rh(1) atom lies anti relative to the cage carbon atom C(1), hence the assignment **5a**-*anti*.

The IR spectrum of the isomeric mixture **5** in the CO stretching region consists of three absorptions at 2024vs,

(8) Allen, F. H.; Brammer, L.; Kennard, O.; Orpen, A. G.; Taylor, R.; Watson, D. G. *J. Chem. Soc., Dalton Trans.* **1989**, S1.

Table 6. Selected Internuclear Distances (Å) and Angles (deg) for [ReRh(CO)$_3$(PMe$_2$Ph)(η^5-C$_5$Me$_5$)(η^5-7-CB$_{10}$H$_{11}$)] (5a-*anti*) with Estimated Standard Deviations in Parentheses

Re(1)−C(3)	1.930(3)	Re(1)−C(4)	1.948(3)	Re(1)−C(2)	1.959(3)	Re(1)−B(2)	2.260(3)
Re(1)−C(1)	2.324(3)	Re(1)−B(5)	2.361(3)	Re(1)−B(3)	2.363(3)	Re(1)−B(4)	2.373(3)
Re(1)−Rh(1)	2.9821(4)	Rh(1)−B(2)	2.307(3)	Rh(1)−P(1)	2.3369(8)	Rh(1)−H(2)	1.66(3)
C(2)−O(2)	1.143(3)	C(3)−O(3)	1.152(3)	C(4)−O(4)	1.143(3)	Rh(1)−C(23)	2.204(2)
Rh(1)−C(21)	2.227(2)	Rh(1)−C(22)	2.235(2)	Rh(1)−C(24)	2.259(3)	Rh(1)−C(25)	2.323(3)

C(3)−Re(1)−Rh(1)	86.86(8)	C(4)−Re(1)−Rh(1)	157.59(8)	C(2)−Re(1)−Rh(1)	77.51(8)
B(2)−Rh(1)−P(1)	100.27(7)	B(2)−Rh(1)−Re(1)	48.55(7)	P(1)−Rh(1)−Re(1)	100.74(2)
O(2)−C(2)−Re(1)	172.6(2)	O(3)−C(3)−Re(1)	174.1(2)	O(4)−C(4)−Re(1)	179.2(3)
B(2)−Re(1)−Rh(1)	49.92(7)	Re(1)−B(2)−Rh(1)	81.54(9)		

Scheme 2. Possible Isomers of Complex 5a[a]

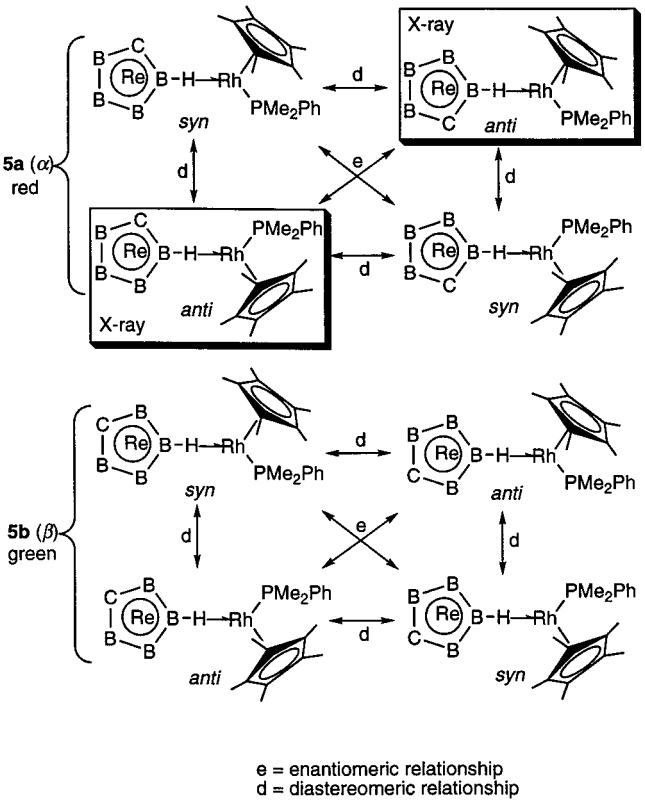

[a] Part of the cage is omitted in all molecules for clarity.

1945s, and 1868m cm^{-1}, a pattern similar to that of **4b**. It was immediately apparent from the ^{31}P{^{1}H} NMR spectrum (Table 3) of **5**, resulting from overnight accumulation of data, that there were several isomers present in solution. This spectrum revealed four doublet signals with a relative peak integral ratio of ca. 1:10:70:30. As Scheme 2 shows, this is in accordance with the fact that it is possible to generate four diastereomeric pairs of enantiomers for complex **5**. This complication arises out of two distinct isomeric variations: (i) the involvement of B$_\alpha$−H or B$_\beta$−H bonds in the B−H⇀Rh three-center two-electron system leading to complexes **5a** or **5b**, respectively; (ii) the relative disposition in either **5a** or **5b** of the η^5-C$_5$Me$_5$ ligand with respect to the cage carbon atom as syn or anti. Thus, the X-ray structure corresponds to the two enantiomers of **5a**-*anti*, and these are highlighted in Scheme 2 by shadow box outlines; both enantiomers are present in the crystal structure as dictated by the achiral space group $P\bar{1}$. We infer from these results and from the rhenium−iridium work to be discussed shortly that the red material consists of the α-series of isomers **5a** and the green material contains the β-bonded isomers **5b**. On the basis of additional observations during the chromatography (i.e., more red than green compound formed), the signal at δ 1.5 in the ^{31}P{^{1}H} NMR spectrum of **5** must correspond to the major enantiomeric pair of isomers of **5a**, tentatively assigned as **5a**-*anti* as found in the X-ray structure. The doublet peak at δ −0.1 is most likely due to one of the green isomers of **5b** (hereafter designated **5b**-*syn*/*anti*), although it is not possible to specifically assign this or the remaining two weak signals (δ 12.9 and 5.8) without direct structural proof.

The ^{31}P{^{1}H} NMR spectrum remained broadly unaffected by lowering the temperature to −90 °C, with minor adjustment in the equilibrium between all four diastereotopic pairs of enantiomers. The ^{11}B{^{1}H} NMR spectrum of **5** displays two low-field signals at δ 22.0 and 22.5 (ca. 2:1) arising from the enantiomeric pair of **5a**-*anti* (major) and from one pair of **5b**-*syn*/*anti* (minor), respectively. These signals are due to the *B*−H⇀Rh boron nuclei, this being verified by running a fully coupled ^{11}B NMR spectrum of **5**. These peaks broaden slightly in comparison with the other signals, but a ^{1}H−^{11}B coupling, normally expected to lie in the range 60−90 Hz for this type of system,[5b] could not be resolved. The remaining two enantiomeric pairs of isomers (which must include **5a**-*syn* and the other isomeric pair **5b**-*anti*/*syn*) are not present in sufficient quantity in solution to give rise to observable resonances in this spectrum. The ^{1}H NMR spectrum of **5** (Table 2) was also informative with two broad high-field peaks for the B−H⇀Rh groups at δ −10.47 (**5a**-*anti*) and −11.26 (**5b**-*syn*/*anti*), having a peak integral ratio of ca. 2:1. No other peaks in this region (δ < −2.00) could be identified. The cage CH protons gave rise to broad peaks at δ 1.96 (**5a**-*anti*) and 2.11 (**5b**-*syn*/*anti*), and in particular, the diastereotopic methyls of the PMe$_2$Ph ligands in **5a**-*anti* produce two doublet resonances at δ 1.50 and 1.85 (J(PH) = 10 and 10 Hz) while those of **5b**-*syn*/*anti* gave doublets at δ 1.70 and 2.00 (J(PH) = 10 and 11 Hz, respectively). Assignments are based on the relative peak intensities of the major red complex **5a**. The ^{13}C{^{1}H} NMR spectrum did not reveal all of the expected signals due to the carbonyl carbon nuclei with just two observable peaks, chiefly because of poor complex solubility. The major enantiomeric pair **5a**-*anti* gives rise to two η^5-C$_5$Me$_5$ signals (δ 10.7 (C$_5$*Me*$_5$) and 106.2 (dd, *C*$_5$Me$_5$, J(PC) = 5, J(RhC) = 2 Hz)) and two doublets as a result of the inequivalent PMe groups (δ 13.7 (J(PC) = 28) and 20.8 (J(PC) = 27 Hz)). The minor green complex **5b**-*syn*/*anti* is responsible for a similar set of smaller peaks (Table 2). Again, the remaining two minor enantiomeric pairs of isomers (**5a**-*syn* and **5b**-*anti*/*syn*) did not produce observable resonances in this spectrum.

With the availability of a complete X-ray-determined

Table 7. UV−Vis Spectral Data for Complexes 4b and 5[a]

4b			5		
λ_{max}	ϵ_o[b]	ϵ_r[c]	λ_{max}	ϵ_o[b]	ϵ_r[c]
604	0.17	0.11	558	0.50	0.17
412	0.57	0.39	408	1.18	0.40
324	0.52	0.35	310	1.31	0.44
256	1.48	1.00	250	2.99	1.00
230	1.43	0.97	236	2.92	0.98

[a] Measured in CH_2Cl_2. [b] ϵ_o = measured absorbance. [c] $\epsilon_r = \epsilon_o/\epsilon_{o,max}$, where $\epsilon_{o,max}$ = measured absorbance of largest peak.

structure of **5a**-*anti* and an appreciation of all the isomers which can be generated for complex **5**, the formation of and NMR data for complex **4b** can be understood. In this case, only a green material was produced. The $^{31}P\{^1H\}$ NMR spectrum of this product consisted of two doublets at δ −11.3 (J(RhP) = 145) and −13.1 (J(RhP) = 150 Hz) which, immediately following chromatography, were present at a peak integral ratio of 5:1. However, after stirring a CH_2Cl_2 solution for an additional 5 days, this ratio adjusted to 1:1. A similar situation occurred when measuring the $^{11}B\{^1H\}$ and ^{11}B NMR spectra. Initially, these revealed a pair of low-field resonances at δ 24.6 and 21.2 (peak integral ratio 5:1) assignable to the *B*−H⇀Rh boron nuclei. After stirring in CH_2Cl_2 for 5 days, these peaks integrated with a ratio of 1:1 also. The ^1H NMR spectrum of **4b** displayed the customary high-field broad signals at δ −10.70 and −11.56 (initial peak integral ratio, 5:1; after 5 days, 1:1). Unfortunately, in neither the ^1H nor the ^{11}B NMR spectra did the signals due to the relevant *B*−*H*⇀Rh nuclei reveal measurable resolved $^{11}B-^1H$ coupling constants. However, there is little doubt as to the assignment; the ^{11}B spectral low-field signals, in particular, do not show $^1H-^{11}B$ coupling greater than 100 Hz, as is typical for terminal B−H bonds,[5b] but appear as broad signals in the fully coupled ^{11}B NMR spectrum. The remaining signals in the ^1H and $^{13}C\{^1H\}$ NMR spectra were as expected, although the very low solubility of the sample did not allow some resonances due to CO and cage carbon nuclei to be observed. It is, thus, apparent that this green material comprises a mixture of the syn and anti isomers of complex **4b**, where the B_β−H bond takes part in agostic bonding to the rhodium atom. Furthermore, since no red compound could be detected by chromatographic analysis, there would seem to be no formation of **4a**, an analogue of the complex **5a**.

The UV−vis spectra of CH_2Cl_2 solutions of **4b** and **5** were measured (Table 7) and were almost identical in form. That of **5** confirmed the predominance in solution of the red complex **5a** with absorptions in the visible region at 408 and 558 nm, while that of **4b** displayed notable broad peaks in the same region at 412 and 604 nm, accounting for the green color. Thus, the discrepancy in color between **5a** and **4b** is due to a subtle yet significant difference (ca. 50 nm) in the longest wavelength d → π^* transitions of these complexes. Transitions arising from the minor green complex **5b** in the compound **5** mixture are presumably masked by the much larger broad absorptions due to **5a**. It is interesting that these rhenium−rhodium systems seem to be particularly electronically sensitive to the nature of the $B_{\alpha/\beta}$−H⇀Rh agostic bonds, when they are otherwise structurally very similar. Attempts to form a stable adduct by addition of $PMePh_2$ to **3a** for the purpose of further analysis and comparison of this type of complex were unsuccessful. This may be due to likely steric congestion, which would result in the target complex.

Synthesis of **3b** in situ at low temperatures followed by treatment with phosphines PR_3 (PR_3 = PMe_3, PMe_2Ph) yielded the rhenium−iridium complexes $[ReIr(CO)_3(PR_3)(\eta^5\text{-}C_5Me_5)(\eta^5\text{-}7\text{-}CB_{10}H_{11})]$ (PR_3 = PMe_3 (**6**), PMe_2Ph (**7**)). From both syntheses it was possible to chromatographically separate mixtures of two isomers formed, one orange (**6a**/**7a**) and the other purple (**6b**/**7b**). Single crystals were grown of **6a** and **7b**, and the X-ray structure determinations of these complexes will be discussed prior to evaluation of the NMR data. Selected bond lengths and angles are given in Table 8 (**6a**) and Table 9 (**7b**), and the molecules are shown in Figures 3 (**6a**) and 4 (**7b**).

There are very few previously recorded X-ray structural characterizations of binuclear rhenium−iridium organometallic complexes: $[ReIr(\mu\text{-}CO)_2(CO)_2(\eta^5\text{-}C_5H_5)(\eta^5\text{-}C_5Me_5)]$[9a] contains a Re−Ir bond (2.8081(6) Å) bridged by two CO ligands and $[ReIr\{\mu\text{-}P(C_6H_{11})_2\}_2(CO)_4\{P(C_6H_{11})_3\}_2]$[9b] has a Re−Ir contact of 2.9117(7) Å. The Re−Ir bond lengths of **6a** (2.9013(6) Å) and **7b** (2.9248(6) Å) are therefore unsurprising.

Complex **6a** is structurally very similar to **5a**. The *nido*-7-$CB_{10}H_{11}$ cage is η^5-coordinated to the rhenium atom and also bonded to iridium via a B(2)−H⇀Ir system, i.e., a B_α boron atom partakes in agostic bonding (B(2)−Ir 2.317(11) Å). The agostic proton bound to B(2) was unfortunately not located, although its presence was fully verified by the NMR spectra. The η^5-C_5Me_5 ligand, which lies anti to the cage carbon C(1) (giving a structure designation **6a**-*anti*), is slightly slipped in a direction away from the phosphorus atom (Ir−C(21) 2.207(10) Å, Ir−C(22) 2.212(11) Å, Ir−C(23) 2.264(9) Å, Ir−C(24) 2.249(10) Å, Ir−C(25) 2.274(10) Å). While PMe_3 is one of the sterically less-demanding phosphine ligands (Tolman cone angle, θ_T = 118°),[10] it is a strong σ-donor, and along with the donor capacities of the bulky η^5-C_5Me_5 and B−H⇀Ir groups, there may be a substantial build-up of electron density on the already electron-rich iridium atom. It is, therefore, not surprising that there is some minor slippage of the pentamethylcyclopentadienyl ring. This phenomenon may also be responsible for the tendency of one of the CO ligands toward a semibridging Re−C(O)···Ir situation (Re−C(3)−O(3) 166.5(9)°) (Figure 3), although the carbonyl carbon C(3) is only weakly bound to the iridium atom (Ir···C(3) 2.66 Å). The remaining two Re−CO groups are near-linear (Re−C(2)−O(2) 176.0(13)°, Re−C(4)−O(4) 174.6(9)°). The Ir−P bond length (2.341(3) Å) is almost identical with the average found for several Ir−PMe_3 complexes (2.323 Å).[8]

The gross structural features of **7b** (Figure 4 and Table 9) bear resemblance to both complexes **5a**-*anti* and **6a**-*anti* with two substantial differences: (i) the agostic bridge system B(3)−H(3)⇀Ir employs a B_β−H bond (Re−B(3) 2.237(4) Å, Ir−B(3) 2.320(4) Å), (ii) the

(9) (a) Zhuang, J.-M.; Batchelor, R. J.; Einstein, F. W. B.; Jones, R. H.; Hader, R.; Sutton, D. *Organometallics* **1990**, *9*, 2723. (b) Baker, R. T.; Calabrese, J. C.; Glassman, T. E. *Organometallics* **1988**, *7*, 1889.
(10) Tolman, C. A. *Chem. Rev.* **1977**, *77*, 313.

Table 8. Selected Internuclear Distances (Å) and Angles (deg) for $[ReIr(CO)_3(PMe_3)(\eta^5\text{-}C_5Me_5)(\eta^5\text{-}7\text{-}CB_{10}H_{11})]$ (6a-*anti*) with Estimated Standard Deviations in Parentheses

Ir−B(2)	2.317(11)	Ir−P	2.341(3)	Ir−Re	2.9013(6)	Re−C(4)	1.921(14)
Re−C(2)	1.967(14)	Re−C(3)	1.966(12)	Re−B(2)	2.203(12)	Re−B(3)	2.368(12)
Re−C(1)	2.363(11)	Re−B(5)	2.386(12)	Re−B(4)	2.403(11)	C(2)−O(2)	1.14(2)
C(3)−O(3)	1.169(13)	C(4)−O(4)	1.148(14)	Ir−C(22)	2.212(11)	Ir−C(21)	2.207(10)
Ir−C(24)	2.249(10)	Ir−C(23)	2.264(9)	Ir−C(25)	2.274(10)		

C(4)−Re−Ir	101.3(3)	C(2)−Re−Ir	143.0(4)	C(3)−Re−Ir	62.8(3)
B(2)−Ir−P	95.4(3)	B(2)−Ir−Re	48.4(3)	P−Ir−Re	97.28(7)
B(2)−Re−Ir	51.8(3)	Re−B(2)−Ir	79.8(4)	O(2)−C(2)−Re	176.0(13)
O(3)−C(3)−Re	166.5(9)	O(4)−C(4)−Re	174.6(9)		

Table 9. Selected Internuclear Distances (Å) and Angles (deg) for $[ReIr(CO)_3(PMe_2Ph)(\eta^5\text{-}C_5Me_5)(\eta^5\text{-}7\text{-}CB_{10}H_{11})]$ (7b-*syn*) with Estimated Standard Deviations in Parentheses

Ir−C(25)	2.195(3)	Ir−C(22)	2.234(3)	Ir−C(21)	2.241(3)	Ir−C(24)	2.280(3)
Ir−C(23)	2.286(3)	Ir−B(3)	2.320(4)	Ir−P	2.3417(10)	Ir···C(4)	2.557(4)
Ir−Re	2.9248(6)	Ir−H(3)	1.44(5)	Re−C(3)	1.932(4)	Re−C(2)	1.939(4)
Re−C(4)	1.949(4)	Re−B(3)	2.237(4)	Re−B(2)	2.323(5)	Re−C(1)	2.381(4)
Re−B(4)	2.383(4)	Re−B(5)	2.392(4)	C(2)−O(2)	1.140(5)	C(3)−O(3)	1.145(4)
C(4)−O(4)	1.163(4)						

B(3)−Ir−P	95.18(11)	B(3)−Ir−C(4)	88.24(13)	P−Ir−C(4)	79.85(9)
B(3)−Ir−Re	48.84(10)	P−Ir−Re	94.98(3)	C(4)−Ir−Re	40.97(9)
C(3)−Re−Ir	107.13(11)	C(2)−Re−Ir	131.33(13)	C(4)−Re−Ir	59.33(11)
B(3)−Re−Ir	51.32(10)	O(2)−C(2)−Re	175.7(4)	O(3)−C(3)−Re	175.1(3)
O(4)−C(4)−Re	164.8(3)	O(4)−C(4)−Ir	115.4(3)	Re−C(4)−Ir	79.69(14)
Re−B(3)−Ir	79.84(13)				

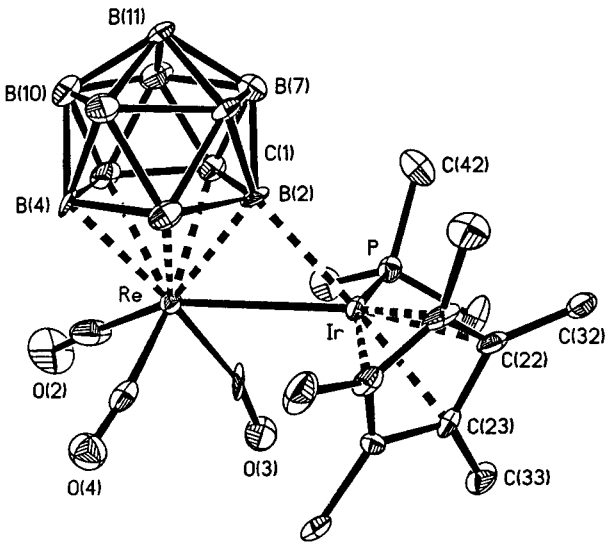

Figure 3. Structure of $[ReIr(CO)_3(PMe_3)(\eta^5\text{-}C_5Me_5)(\eta^5\text{-}7\text{-}CB_{10}H_{11})]$ (**6a**-*anti*), showing the crystallographic labeling scheme. Thermal ellipsoids are shown at the 40% probability level. Hydrogen atoms are omitted for clarity.

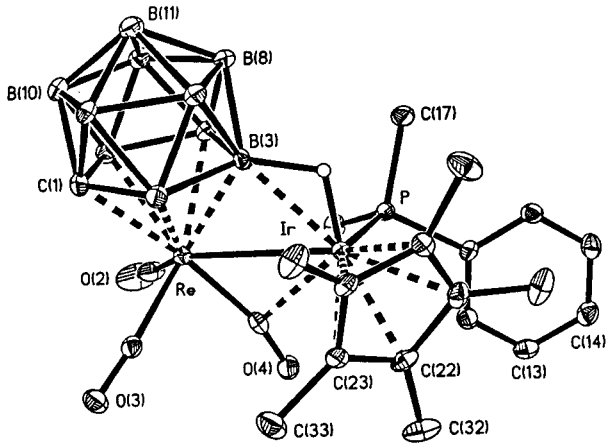

Figure 4. Structure of $[ReRh(CO)_3(PMe_2Ph)(\eta^5\text{-}C_5Me_5)(\eta^5\text{-}7\text{-}CB_{10}H_{11})]$ (**7b**-*syn*), showing the crystallographic labeling scheme. Thermal ellipsoids are shown at the 40% probability level. Only the agostic hydrogen atom is shown for clarity.

particular isomer studied here has the η^5-C_5Me_5 ligand lying syn to the cage carbon C(1), i.e., the complex is designated **7b**-*syn*. The Ir−P bond length (2.3417(10) Å) is comparable with the average found in other complexes which possess Ir−PMe_2Ph bonds (2.319 Å).[8] The η^5-C_5Me_5 ring is partially slipped as in **5a**-*anti* and **6b**-*anti* (Ir−C(21) 2.241(3) Å, Ir−C(22) 2.234(3) Å, Ir−C(23) 2.286(3) Å, Ir−C(24) 2.280(3) Å, Ir−C(25) 2.195(3) Å). The carbonyl C(4)−O(4) very weakly semibridges the Re−Ir bond (Re−C(4) 1.949(4) Å, Ir···C(4) 2.557(4) Å, Re−C(4)−O(4) 164.8(3)°, Ir−C(4)−O(4) 115.4(3)°). As with **5a**-*anti* and **6a**-*anti*, the small ring-slippage in **7b**-*syn* may be a combination of the steric demands of the ligands around the iridium atom and the electron density accretion at the iridium due to the presence of several strong electron donors. The latter would also account for the weak semibridging nature of the C(4)−O(4) ligand. From these structure determinations, it is reasonable to declare that the orange compounds **6a** and **7a** contain B_α−H⇀Ir-bonded complexes and the purple compounds (**6b** and **7b**) are composed of B_β−H⇀Ir-bonded isomers.

In the synthesis of complex **6**, there was a clear preference for the formation **6b** over **6a** (4:1), but the reverse was true with regard to complex **7**, where **7a** was the major product over **7b** (3:1). The IR spectra in the CO stretching region of the rhenium−iridium compounds, **6** and **7**, are similar in form to that of **5**. Notably, in the IR spectra of the complexes which have been characterized structurally by X-ray diffraction are found the lowest frequency ν_{max}(CO) absorptions (1888m (**6a**) and 1865m cm^{-1} (**7b**)). These values, the latter in particular, border on the frequency range for bridging CO ligands in transition-metal cluster molecules and would seem to correlate with the findings of the crystal structure determinations, especially that of **7b**.

The NMR measurements on the orange complex **6a** revealed the presence of two isomers or more correctly

two diastereomeric pairs of enantiomers. The ^{1}H NMR spectrum (Table 2) shows one broad resonance at δ −13.54, which corresponds to the B_α−*H*⇀Ir nucleus in the major enantiomeric pair of isomers of **6a** in solution. There are the expected set of signals due to the PMe_3 and η^5-C_5Me_5 ligands for both sets of isomers, and broad singlets due to the cage CH protons at δ 2.10 and 2.18 (4:1) are also observed. The $^{11}B\{^1H\}$ NMR spectrum (Table 3) displays diagnostic signals for the B_α−H⇀Ir boron nuclei at δ 23.4 and 21.3 (4:1).[5b] No $^1H-^{11}B$ coupling could be resolved for these two resonances in a fully coupled ^{11}B NMR spectrum, but the assignment is unquestionable. The $^{31}P\{^1H\}$ NMR spectrum (Table 3) shows two singlets at δ −47.2 and −44.8, once again in a ratio 4:1, while the $^{13}C\{^1H\}$ NMR spectrum revealed resonances due to the carbonyl carbon nuclei at δ 196.9 and 195.6. The latter signal is broad and most likely arises from the fortuitous overlap of two separate peaks. The remaining peaks in this spectrum are as expected. It is possible that the major enantiomeric pair of isomers in **6a** is that observed in the X-ray structure, i.e., **6a**-*anti*. However, without unambiguous detailed X-ray structures of all isomers concerned, this remains inconclusive; such a pursuit would not be practical.

The NMR spectra of the purple complex **6b** are dominated by peaks due to a major isomer with a broad resonance in the ^{1}H NMR spectrum at δ −14.82 and doublets arising from the PMe_3 and η^5-C_5Me_5 ligands. The diagnostic broad singlet at δ 2.11 due to the cage CH proton was also observed. Very weak peaks were observed for the PMe_3 and η^5-C_5Me_5 ligands of a minor isomer. Due to very low solubility in suitable solvents, a reasonable $^{13}C\{^1H\}$ NMR spectrum was not acquired. The $^{31}P\{^1H\}$ NMR spectrum, however, revealed the presence of both diastereomeric pairs of enantiomers with singlets at δ −43.0 and −42.1 (9:1). The $^{11}B\{^1H\}$ NMR spectrum showed the characteristic[5b] low-field peak at δ 25.1 for the B_α−H⇀Ir boron nucleus of the major isomer, with no observable corresponding resonance due to the minor isomer, most likely because of the poor solubility of the complex. Once again, both syn an anti isomers exist in solutions of **6b**, but assignment of major and minor species is impossible: both are unsymmetrical and would give rise to similar sets of NMR data.

As with the complexes **6**, the B_α−H⇀Ir (orange) and B_β−H⇀Ir (purple) bonded isomers of compound **7** were successfully separated on a silica gel chromatography column. Complex **7a** was composed of a mixture of two isomeric species, as indicated by the $^{31}P\{^1H\}$ NMR spectrum (Table 3, δ −31.8 and −30.3 (7:1)). This was also reflected in the $^{11}B\{^1H\}$ NMR spectrum with peaks at δ 24.8 and 25.5 (7:1) due to the B_α−H⇀Ir boron nuclei. Only one broad B_α−H⇀Ir proton resonance was seen in the ^{1}H NMR spectrum (δ −13.30) for the major species of **7a**, the relevant peak for the minor complex either being masked or too weak to be observed. The latter, however, did produce a doublet at δ 1.64 (C_5Me_5, J(PH) = 3) and two doublets at δ 1.89 and 2.08 (J(PH) = 11 and 11 Hz) resulting from the diastereotopic methyl groups of the PMe_2Ph ligand. These signals may be compared with those for the major species present at δ 1.79 (d, C_5Me_5, J(PH) = 2) and at 1.54 and 1.98 (d × 2, PMe, J(PH) = 10 and 10 Hz). Solubility was yet again a hindrance to the observation of all carbon nuclei in the $^{13}C\{^1H\}$ NMR spectrum of **7a**, with only one peak positively identified as resulting from carbonyl carbon nuclei (δ 195.2). Signals at δ 102.2 (minor) and 102.1 (major) and at 10.2 (major) and 10.0 (minor) confirm the presence of the η^5-C_5Me_5 ligand, while the P*Me*$_2$Ph groups of the major species are also responsible for two doublets at δ 13.9 and 22.3 (J(PC) = 36 and 37 Hz, respectively).

Complex **7b**, whose structural features have been discussed above (Figure 4), interestingly consists only of the syn species in solution. Hence, the $^{31}P\{^1H\}$ NMR spectrum (Table 3) displays only one singlet and the $^{11}B\{^1H\}$ NMR spectrum one low-field signal due to the B_β−H⇀Ir system. The ^{1}H NMR spectrum was straightforward with a characteristic broad high-field B_β−*H*⇀Ir proton resonance at δ −14.49, a doublet at δ 1.70 (C_5Me_5, J(PH) = 2), and two doublets at δ 1.88 and 2.02 (PMe × 2, J(PH) = 11 and 11 Hz). The $^{13}C\{^1H\}$ NMR spectrum was as expected (Table 2).

A low-energy exchange process between B_α−H⇀M and B_β−H⇀M bonded moieties in solution has been documented previously for metallacarborane complexes of the dicarbollide ligands $[nido\text{-}7,8\text{-}R_2\text{-}7,8\text{-}C_2B_9H_9]^{2-}$ (R = H, Me)[11] and more recently for the $[nido\text{-}7\text{-}CB_{10}H_{11}]^{3-}$ ligand in rhenacarborane−palladium work.[3b] To observe both isomeric forms simultaneously in a binuclear metal complex, as in **6** or **7**, and then to cleanly separate these isomers by chromatography is unprecedented in this field. To establish whether the interconversions **6a** ↔ **6b** or **7a** ↔ **7b** were feasible at elevated temperatures, benzene suspensions of the complexes were refluxed for 24 h and then their NMR spectra measured. Complex **6b** was unaffected, but **6a** underwent a ca. 15% conversion into **6b** in this time, along with a small amount of decomposition. Complexes **7a** and **7b** showed no propensity to interconvert under these conditions.

Conclusions

The new complex **1a** is clearly a versatile reagent for synthesis and has proven useful in groundbreaking work to create new compounds with metal−metal bonds. The novel rhenacarborane−rhodium complex **3a** is a highly dynamic molecule in solution. Addition of phosphines to **3a** forms stable adducts (**4b** and **5**) and anchors the Rh(η^5-C_5Me_5) unit on to the rhenium atom, although the nature of the resulting product is sensitive to the phosphine used. With the analogous rhenium−iridium complexes **6** and **7**, the presence of the phosphine (PMe_3 or PMe_2Ph) not only fixes the Re−Ir bond into place, but also effectively inhibits the exchange between B_α−H⇀Ir and B_β−H⇀Ir systems at ambient temperatures. We anticipate further advances will be made in this area of research.

Experimental Section

General Considerations. All experiments were conducted under an atmosphere of dry nitrogen using Schlenk tube techniques. Solvents were freshly distilled under nitrogen

(11) (a) Jeffery, J. C.; Ruiz, M. A.; Sherwood, P.; Stone, F. G. A. *J. Chem. Soc., Dalton Trans.* **1989**, 1845. (b) Hendershot, S. L.; Jeffery, J. C.; Jelliss, P. A.; Mullica, D. F.; Sappenfield, E. L.; Stone, F. G. A. *Inorg. Chem.* **1996**, *35*, 6561.

Table 10. Data for X-ray Crystal Structure Analyses

	3a	**5a**-*anti*	**6a**-*anti*	**7b**-*syn*
cryst dimens/mm	0.20 × 0.30 × 0.40	0.10 × 0.26 × 0.45	0.20 × 0.35 × 0.37	0.20 × 0.22 × 0.38
formula	$C_{14}H_{26}B_{10}O_3ReRh$	$C_{22}H_{37}B_{10}O_3PReRh{\cdot}CH_2Cl_2$	$C_{17}H_{35}B_{10}IrO_3PRe$	$C_{22}H_{37}B_{10}IrO_3PRe$
M_r	639.56	862.62	804.92	866.99
cryst color, shape	red-brown, prism	red, plate	orange, prism	purple, prism
cryst syst	triclinic	monoclinic	monoclinic	triclinic
space group	$P\bar{1}$	$P2_1/c$	$P2_1/n$	$P\bar{1}$
T/K	173	173	173	173
a/Å	15.210(2)	13.642(3)	9.833(2)	9.800(2)
b/Å	15.569(2)	14.618(2)	11.8491(14)	10.889(3)
c/Å	16.247(2)	16.274(2)	22.623(4)	14.829(3)
α/deg	114.074(7)			72.966(14)
β/deg	94.308(8)	98.635(13)	100.96(2)	78.017(12)
γ/deg	104.421(9)			77.705(10)
V/Å^3	3333.5(6)	3208.7(8)	2587.8(8)	1460.5(6)
Z	6	4	4	2
d_{calcd}/g cm^{-3}	1.912	1.786	2.066	1.971
μ(Mo Kα)/mm^{-1}	6.197	4.526	9.891	8.771
F(000)/e	1824	1680	1512	820
2θ range/deg	2.8−55.0	3.0−55.0	2.6−45.0	2.0−55.0
data frame collcn time (per frame/s, overall/h)	20, ca. 10	20, ca. 10	10, ca. 6	10, ca. 6
no. of rflns measd	21 183	20 134	10 601	15 098
no. of indep rflns	14 525	7335	3392	6611
refinement method	full-matrix least-squares on all F^2 data	full-matrix least-squares on all F^2 data	full-matrix least-squares on all F^2 data	full-matrix least-squares on all F^2 data
final residuals	wR_2 = 0.081[a] (R_1 = 0.035)[b]	wR_2 = 0.047[a] (R_1 = 0.020)[b]	wR_2 = 0.096[a] (R_1 = 0.037)[b]	wR_2 = 0.042[a] (R_1 = 0.019)[b]
weighting factors	a = 0.0303; b = 0.0[a]	a = 0.0233; b = 0.0[a]	a = 0.0545; b = 0.0[a]	a = 0.0139; b = 0.0[a]
goodness of fit on F^2	0.873	0.89	1.039	0.963
final electron density diff features (max/min)/e Å^{-3}	2.353, −2.057	0.79, −0.76	2.884, −1.491	1.08, −1.11

[a] Structure was refined on F_o^2 using all data: w$R_2 = [\sum[w(F_o^2 - F_c^2)^2]/\sum w(F_o^2)^2]^{1/2}$, where $w^{-1} = [\sigma^2(F_o^2) + (aP)^2 + bP]$ and $P = [\max(F_o^2,0) + 2F_c^2]/3$. [b] The value in parentheses is given for comparison with refinements based on F_o with a typical threshold of $F_o > 4\sigma(F_o)$ and $R_1 = \sum||F_o| - |F_c||/\sum|F_o|$ and $w^{-1} = [\sigma^2(F_o) + gF_o^2]$.

from appropriate drying agents before use. Light petroleum refers to that fraction of boiling point 40−60 °C. Chromatography columns (ca. 60 cm long and 1 cm in diameter) were packed with silica gel (Aldrich, 70−230 mesh). The NMR measurements were recorded at the following frequencies: ^{1}H at 360.13, ^{13}C at 90.56, ^{11}B at 115.55, and ^{31}P at 145.78 MHz. The reagents $[N(PPh_3)_2]_2[Re(CO)_3(\eta^5\text{-}7\text{-}CB_{10}H_{11})]$ (**1a**)[3b] and $[M(NCMe)_3(\eta^5\text{-}C_5Me_5)][BF_4]_2$ (M = Rh, Ir)[12] were made as previously described. The ligands PMe_3 and PMe_2Ph were used as purchased from Aldrich.

Synthesis of $[ReRh(CO)_3(\eta^5\text{-}C_5Me_5)(\eta^5\text{-}7\text{-}CB_{10}H_{11})]$. A mixture of the compounds **1a** (1.00 g, 0.68 mmol) and $[Rh(NCMe)_3(\eta^5\text{-}C_5Me_5)][BF_4]_2$ (0.36 g, 0.67 mmol) was treated with MeCN (30 mL), and the solution, which turns instantly red-brown, was stirred for ca. 15 min. Solvent was removed in vacuo, and CH_2Cl_2 (3 mL) was added, followed by chromatographic purification. Elution with CH_2Cl_2−light petroleum (7:3) removed a deep red-brown fraction. Crystallization from CH_2Cl_2−light petroleum (15 mL, 1:3) gave red-brown microcrystals of $[ReRh(CO)_3(\eta^5\text{-}C_5Me_5)(\eta^5\text{-}7\text{-}CB_{10}H_{11})]$ (**3a**) (0.35 g).

Syntheses of the Complexes $[ReRh(CO)_3(PR_3)(\eta^5\text{-}C_5Me_5)(\eta^5\text{-}7\text{-}CB_{10}H_{11})]$. (i) A solution of **3a** (0.05 g, 0.08 mmol) in CH_2Cl_2 (10 mL) was cooled to −10 °C. A solution of PMe_3 (80 μL, 1.0 M in THF, 0.08 mmol) was added to CH_2Cl_2 (10 mL) in a dropping funnel, and this was added dropwise to the cold solution of **3a** over a period of ca. 0.5 h. The solution turned deep green in this time. The reaction was stirred for a further 0.5 h, after which time the volume was reduced in vacuo to ca. 4 mL. This was chromatographed, and a deep green fraction was eluted with CH_2Cl_2−light petroleum (3:2). Crystallization from CH_2Cl_2−light petroleum (12 mL, 1:5) gave dark green microcrystals of $[ReRh(CO)_3(PMe_3)(\eta^5\text{-}C_5Me_5)(\eta^5\text{-}7\text{-}CB_{10}H_{11})]$ (**4b**) (0.04 g).

(ii) A solution of **3a** (0.09 g, 0.14 mmol) in CH_2Cl_2 (10 mL) was cooled to −78 °C and stirred. A solution of PMe_2Ph (20 μL, 0.14 mmol) in CH_2Cl_2 (10 mL) was added via a dropping funnel over a 20 min period. After the addition was complete, the reaction mixture was allowed to warm to room temperature to give a green-brown solution and stirred overnight. At this point, no further changes were registered upon IR measurement and TLC (silica gel plate, 250 μm layer, CH_2Cl_2−light petroleum (1:1)) revealed two bands: a green fraction running just ahead of a red-brown band. Solvent was reduced in volume in vacuo to ca. 4 mL, and the solution was chromatographed at −30 °C. Initial elution with CH_2Cl_2−light petroleum (1:1) removed a deep green fraction. A red-brown band was then eluted from the column with CH_2Cl_2−light petroleum (4:1). However, after removal from the chromatography column, both fractions reverted to the same green-brown color within 1−2 min. IR, NMR, and microanalytical analysis confirmed that both fractions were of the same composition. Removal of solvent in vacuo and crystallization from CH_2Cl_2−light petroleum (10 mL, 1:4) gave a mixture of red and green microcrystals of $[ReRh(CO)_3(PMe_2Ph)(\eta^5\text{-}C_5Me_5)(\eta^5\text{-}7\text{-}CB_{10}H_{11})]$ (**5**) (0.09 g)

Synthesis of the Isomers of $[ReIr(CO)_3(PR_3)(\eta^5\text{-}C_5Me_5)(\eta^5\text{-}7\text{-}CB_{10}H_{11})]$. (i) A solution of **1a** (0.2 g, 0.14 mmol) in CH_2Cl_2 (10 mL) was cooled to −30 °C. From a dropping funnel, a solution of $[Ir(NCMe)_3(\eta^5\text{-}C_5Me_5)][BF_4]_2$ (0.09 g, 0.14 mmol) in CH_2Cl_2 (10 mL) was added slowly. To make sure no iridium reactant remained in the funnel, a small amount of neat CH_2Cl_2 (2 mL) was washed through. The reaction mixture was warmed to 0 °C, stirred for ca. 15 min, and then cooled to −78 °C. A solution of PMe_3 (140 μL, 1.0 M in THF, 0.14 mmol) was added to CH_2Cl_2 (10 mL), placed in the same dropping funnel, and then added to the reaction mixture over the course of ca. 20 min. After the mixture was gradually warmed to room temperature, it was stirred overnight. Solvent was reduced in volume in vacuo to ca. 5 mL, and the solution was chromatographed. Initial elution with CH_2Cl_2−light petroleum (3:2) removed a purple fraction. Removal of solvent in vacuo and crystallization from CH_2Cl_2−light petroleum (10 mL, 1:1) gave purple microcrystals of the β-isomer of $[ReIr(CO)_3(PMe_3)(\eta^5\text{-}C_5Me_5)(\eta^5\text{-}7\text{-}CB_{10}H_{11})]$ (**6b**) (0.08 g). Further elution of the chromatography column with CH_2Cl_2−light petroleum (4:1) removed an orange fraction. Crystallization from CH_2Cl_2−light petroleum (8 mL, 3:1) gave orange microcrystals of the α-isomer of $[ReIr(CO)_3(PMe_3)(\eta^5\text{-}C_5Me_5)(\eta^5\text{-}7\text{-}CB_{10}H_{11})]$ (**6a**) (0.02 g)

(ii) Using a similar procedure, **1a** (0.20 g, 0.14 mmol), $[Ir(NCMe)_3(\eta^5\text{-}C_5Me_5)][BF_4]_2$ (0.09 g, 0.14 mmol), and PMe_2Ph (20 μL, 0.14 mmol) in CH_2Cl_2 (30 mL) gave purple microcrystals of the β-isomer of $[ReIr(CO)_3(PMe_2Ph)(\eta^5\text{-}C_5Me_5)(\eta^5\text{-}7\text{-}CB_{10}H_{11})]$ (**7b**) (0.02 g) and orange microcrystals of the α-isomer of $[ReIr(CO)_3(PMe_2Ph)(\eta^5\text{-}C_5Me_5)(\eta^5\text{-}7\text{-}CB_{10}H_{11})]$ (**7a**) (0.06 g).

Crystal Structure Determinations and Refinements. Crystals of **3a** were grown by diffusion of *n*-hexane into a CH_2Cl_2 solution of the complex, while those of **5a**-*anti*, **6a**-*anti*, and **7b**-*syn* were grown similarly, but with light petroleum replacing *n*-hexane. Crystals of **5a**-*anti* grow with a molecule of CH_2Cl_2 in the asymmetric unit. All crystals were mounted on glass fibers, and low-temperature data were collected on a Siemens SMART CCD area-detector three-circle diffractometer (Mo Kα X-radiation, graphite monochromator, $\bar{\lambda} = 0.710\ 73$ Å). For three settings of ϕ, narrow data "frames" were collected for 0.3° increments in ω. In all cases, a total of 1271 frames of data were collected, affording rather more than a hemisphere of data for each experiment. It was confirmed that crystal decay had not taken place during the course of the data collections. The substantial redundancy in data allows empirical absorption corrections (SADABS[13]) to be applied using multiple measurements of equivalent reflections. The data frames were integrated using SAINT,[13] and the structures were solved by conventional direct methods and refined by full-matrix least-squares on all F^2 data using Siemens SHELXTL version 5.03.[13] The asymmetric unit of **3a** contains three crystallographically independent molecules of the complex in general positions. For molecule 2 (containing Re(2)Rh(2)), the cage carbon atom could not be unambiguously identified and it is possible that this carbon is disordered over the two sites which are adjacent to the agostic B−H⇀Rh boron atoms. For all structures, the non-hydrogen atoms were refined with anisotropic thermal parameters with the exception of atom B(35) in molecule 3 of **3a** which was found to be unstable under these conditions and was, therefore, restrained to have approximate isotropic character. Cage carbon atoms were identified from the magnitudes of their anisotropic thermal parameters and from a comparison of bond lengths to adjacent boron atoms. With the exception of **6a**-*anti*, all agostic B−H⇀M (Rh, Ir) hydrogen atoms were located and refined. All other hydrogen atoms were included in calculated positions and allowed to ride on the parent boron or carbon atoms with isotropic thermal parameters ($U_{iso} = 1.2 \times U_{iso\ equiv}$ of the parent atom except for Me protons where $U_{iso} = 1.2 \times U_{iso\ equiv}$). The final electron density difference syntheses for **3a** and **6a**-*anti* showed large residual peaks in the vicinity of the transition-metal atoms and reflect the comparatively poor quality of the crystals available for data collection and an inability to completely correct for residual absorption effects. All calculations were carried out on Silicon Graphics Iris, Indigo, or Indy computers and experimental data are recorded in Table 10.

Acknowledgment. We thank the Robert A. Welch Foundation for support (Grant No. AA-1201).

(12) Maitlis, P. M.; Thompson, S. J.; White, C. *J. Chem. Soc., Dalton Trans.* **1977**, 1654.

(13) Siemens X-ray Instruments: Madison, WI, 1995.

Supporting Information Available: Tables of atomic coordinates and *U* values, bond lengths and angles, and anisotropic thermal parameters and ORTEP diagrams for **3a**, **5a**-*anti*, **6a**-*anti*, and **7b**-*syn* (59 pages). Ordering information is given on any current masthead page.

OM9800243